Increase in Axial Compressibility in a Spinning Van der Waals Gas

Yun Liu [1] , **Hao Liu** [1,*] , **Zhen-Guo Fu** [2] **and Weimin Zhou** [3]

1 Department of Applied Physics, School of Physics and Electronics, Hunan University, Changsha 410082, China; yunliu@hnu.edu.cn
2 Dengjiaxian Innovation Research Center, Institute of Applied Physics and Computational Mathematics, Beijing 100088, China; fu_zhenguo@iapcm.ac.cn
3 Science and Technology on Plasma Physics Laboratory, Laser Fusion Research Center, China Academy of Engineering Physics, Mianyang 621900, China; zhouwm@caep.cn
* Correspondence: haoliu@hnu.edu.cn

Abstract: We investigated the adiabatic compression along the axial direction of a spinning Van der Waals gas by applying theoretical analysis and molecular dynamics (MD) simulations. Based on the analytical results, the rotation-induced compressibility increase effect is significant in a Van der Waals gas, while the attraction term in the Van der Waals equation of states (EOS) contributes significantly to the compressibility increase in a spinning system. We conducted MD simulations to the axial compression of a spinning gas, whose state is far from the ideal gas state, and further demonstrated that the rotation-induced compressibility increase effect in a dense state is robust, implying that such a phenomenon can be detected in experiments under high-energy-density conditions.

1. Introduction

High compression of matter is a fundamental subject in the fields of inertial confinement fusion (ICF) [1–4], high-energy-density physics [5,6], and laboratory astrophysics [7], including accretion disks or compact stars [8]. The investigation of the compressibility of a spinning gas may particularly be promising significant in the research in related fields, especially in areas such as the design of Z-pinch experiments [9,10], and the applications of devices to improve the efficiency of engines while reducing pollutants [11,12].

Geyko and Fisch [13] conducted a theoretical study around the axial adiabatic compression of an ideal spinning gas, demonstrating that part of the external pdV work used to compress the gas converts into the rotational kinetic energy E_r of the system during the compression, resulting in lower temperature T and axial pressure p and a softer spinning gas to be compressed.

The ideal gas model is a highly simplified model where interactions between gas molecules are ignored. This raises the question of whether the unusual compressive feature derived from the ideal gas can still be suitable for a nonideal gas. In our previous theoretical work [14], we examined the axial compressibility of a spinning gas using a simple virial equation of states (EOS) and showed that the effect of rotation-induced compressibility increase exists in a spinning nonideal gas with a virial EOS. However, the virial form of EOS can only simply consider the repulsive interactions between gas molecules. In comparison, the Van der Waals EOS includes the modification to the ideal-gas EOS by the repulsive and attractive interactions of gas molecules, so it can better reflect the compressive feature of real gases in a spinning system. Furthermore, as the compression ratio of gas further increases, all the simple theoretical form of EOS will become invalid. The molecular dynamics simulation method can provide an accurate description of the compression process under the conditions far from the ideal gas. Therefore, in order to explore whether the real gas

can have the similar compressive properties in a spinning system, we concentrate on the axial adiabatic compression of a spinning Van der Waals gas with the aid of theoretical analysis and numerical molecule dynamics simulation methods.

To keep the conditions consistent with the previous theoretical work, we consider Geyko's assumptions for the gas compression: (i) the length L of the cylinder is much larger than the radius R of the cylinder so that the end effect (the influence caused by the end surface of the cylinder) can be ignored; (ii) the cylindrical side surface ($r = R$) is smooth and frictionless; (iii) the compression process is quasi-static; and (iv) the gas is in a thermodynamic equilibrium state throughout the compression process.

A dimensionless equation of the density distribution is derived based on the EOS of a Van der Waals gas, as well as the mechanical equilibrium condition. Here, the density distribution form of the Van der Waals gas is represented by three dimensionless parameters that correspond to the intensity of the rotation, repulsive effect (volume effect) of the gas molecules, and attraction between the molecules. We show the influence of each dimensionless parameter on the compressive features of the gas by comparing the variations of the thermodynamic quantities of the system during compression, under different combinations of the initial dimensionless parameters.

Compared with the theoretical method, the molecular dynamics (MD) simulation method can more accurately describe the behaviors of real gases from the perspective of microscopic particle dynamics [15]. Thus, we simulate the axial adiabatic compression of gases with different initial states using the MD method and show that the spinning gas, far from the ideal gas state, would still exhibit an obvious compressibility increase effect, verifying the robustness of this effect in nonideal gases.

The rest of the article is divided into three sections. In Section 2, we present the theoretical analysis based on the EOS of the Van der Waals gas and discuss the numerical results. The details and results of the MD simulation are provided in Section 3. In Section 4, we outline the main conclusions and a short summary of the findings. The definitions of all parameters and their expressions can be found in Table A1 of the Appendix A.

2. Theoretical Analysis

The EOS of a Van der Waals gas is represented by

$$(p + an^2)(1 - bn) = nk_BT, \tag{1}$$

where p, n, and T denote the pressure, number density, and temperature of the gas; k_B is the Boltzmann constant; and parameters a and b correspond to the magnitude of the weak attraction between particles and modification of the molecular volume (thus, b has the dimension of a volume), respectively. In this study, we assume that the values of a and b are constant and do not change with the compression.

Considering the distribution of n in a spinning gas:

$$dp = \left\{ k_BT \left[\frac{1}{1-bn} + \frac{bn}{(1-bn)^2} \right] - 2an \right\} dn, \tag{2}$$

this uses the isothermal approximation. The balance between the centrifugal force dF and dp leads to:

$$\left\{ k_BT \left[\frac{1}{1-bn} + \frac{bn}{(1-bn)^2} \right] - 2an \right\} \frac{dn}{n} = m\omega^2 r dr, \tag{3}$$

where m is the mass of one gas molecule, ω is the angular speed, and r is the radius from the axis of the cylinder. Integration of Equation (3) yields:

$$k_BT \left[ln \frac{n}{n_0} - ln \frac{1-bn}{1-bn_0} + \frac{1}{1-bn} - \frac{1}{1-bn_0} \right] - 2a(n - n_0) = \frac{1}{2}m\omega^2 r^2, \tag{4}$$

where n_0 is the number density at $r = 0$. We introduce the dimensionless parameters α, ζ, and φ to Equation (4) to obtain a dimensionless expression:

$$ln\frac{\tilde{n}}{\tilde{n}_0} - ln\frac{1-\zeta\tilde{n}}{1-\zeta\tilde{n}_0} + \frac{1}{1-\zeta\tilde{n}} - \frac{1}{1-\zeta\tilde{n}_0} - \alpha(\tilde{n} - \tilde{n}_0) = \varphi\tilde{r}^2,\tag{5}$$

where

$$\begin{aligned}
\overline{n} &= \frac{N}{V} = \frac{N}{pR^2L},\\
\tilde{n} &= \frac{n}{\overline{n}},\\
\tilde{r} &= \frac{r}{R},\\
\alpha &= \frac{2a\overline{n}}{k_BT},\\
\zeta &= b\overline{n},\\
\varphi &= \frac{mw^2R^2}{2k_BT}.
\end{aligned}\tag{6}$$

Here, we define N as the total number of particles in the cylinder with volume V, radius R, and height L. Accordingly, $\overline{n}$ is the mean number density of the system, and $\{\tilde{n}, \tilde{r}, \alpha, \zeta, \varphi\}$ is a set of dimensionless parameters denoting, respectively, the number density, cylindrical radius, ratio of the mutual attraction of potential and thermal energies between the gas particles, effect of particle volume (repulsion between the particles), and ratio of the spinning kinetic energy to the thermal energy. We can determine the value of n_0 in Equation (5) using the equation of the normalized condition:

$$\int_0^1 2\tilde{n}(\tilde{r})\tilde{r}d\tilde{r} = 1,\tag{7}$$

this can be applied to Equation (5) to find the distribution of $\tilde{n}(\tilde{r})$. Meanwhile, the dimensionless pressure is given by

$$\tilde{p} = \frac{p}{\overline{n}k_BT} = \frac{\tilde{n}}{1-\zeta\tilde{n}} - \frac{\alpha\tilde{n}^2}{2},\tag{8}$$

whereas the average pressure on the two end surfaces of the cylinder (axial pressure) can be calculated using the equation:

$$\overline{p} = \overline{n}k_BT\int_0^1 \tilde{p}(\tilde{r})2\tilde{r}d\tilde{r}.\tag{9}$$

To ensure that the Van der Waals model can work in the calculations of $\tilde{n}(\tilde{r})$, limiting the range of the dimensionless parameters α and ζ is necessary. Firstly, the value of ζ must not exceed 1; the pressure diverges as ζ approaches 1 and the EOS of a Van der Waals gas is invalid when $\zeta > 1$. Secondly, $\alpha/\zeta < 27/4$ should be satisfied during the calculations to ensure the monotonic relationship between the pressure and the number density. When α/ζ is too large, the system becomes dominated by the attraction term between the particles and undergoes a phase transition from a gaseous to condensed state, which is beyond the scope of the model of the Van der Waals EOS.

Now, we consider a continuous, adiabatic, axial compression process of the gas in the cylinder. All parameters of the system, such as $\overline{n}$, T, and ω, will change accordingly when L is decreased. The relationship between $\overline{n}$ and L is determined by Equation (6), while T and ω vary with L according to the conservation equations of angular momentum and energy. By decomposing the continuous compression process by steps, we can calculate the value of the compression in the spinning gas using these numerical methods.

Suppose that, in a tiny compression, the height of the cylinder changes from L to L' and the values of the system parameters $\overline{n}$, T, and ω to $\overline{n}'$, T', and ω', respectively, the angular momentum of the spinning gas is given by:

$$M = mL\int_0^R 2\pi rdrn(\text{r})\omega r^2 = 2\pi mLR^4\omega\overline{n}\int_0^1 \tilde{n}(\tilde{r})\tilde{r}^3d\tilde{r} = 2mR^2\omega N\int_0^1 \tilde{n}(\tilde{r})\tilde{r}^3d\tilde{r}.\tag{10}$$

The conservation of angular momentum of the system requires that the angular momentum before and after the tiny compression M' to be equal:

$$2mR^2\omega N \int_0^1 \tilde{n}(\tilde{r})\tilde{r}^3 d\tilde{r} = 2mR^2\omega' N \int_0^1 \tilde{n}'(\tilde{r})\tilde{r}^3 d\tilde{r}. \tag{11}$$

The internal energy U could be represented as a function $U(T, V)$. Choosing T and V as the basic state parameters, we can express the full differential of U as:

$$dU = \left(\frac{\partial U}{\partial T}\right)_V dT + \left(\frac{\partial U}{\partial V}\right)_T dV, \tag{12}$$

where the form $(\partial U/\partial T)_V = C_V$, which represents the isometric heat capacity of the gas and could be substituted into the above equation. Meanwhile, the relationship between p and the Helmholtz free energy F is given by

$$-p = \left(\frac{\partial F}{\partial V}\right)_T = \left(\frac{\partial (U - TS)}{\partial V}\right)_T = \left(\frac{\partial U}{\partial V}\right)_T - T\left(\frac{\partial S}{\partial V}\right)_T. \tag{13}$$

Substituting the Maxwell relation $\left(\frac{\partial S}{\partial T}\right)_T = \left(\frac{\partial p}{\partial T}\right)_V$ into Equation (13), we have:

$$\left(\frac{\partial U}{\partial V}\right)_T = T\left(\frac{\partial p}{\partial T}\right)_V - p. \tag{14}$$

Furthermore, substituting Equations (1) and (14) into (12) yields the expression of dU for a Van der Waals gas:

$$dU = C_V dT + aN dn. \tag{15}$$

Assuming that $C_V = 3/2 N k_B$ for a Van der Waals gas is the same as that of an ideal gas, we can integrate Equation (15) to re-express the internal energy U as:

$$U = \frac{3}{2} N k_B T + aN n \tag{16}$$

where the first and second terms correspond to the thermal energy E_t and potential energy E_p, respectively. Considering the density distribution in the spinning gas, the total potential energy is an integral expression:

$$E_p = \int_0^R an^2 L2\pi r \, dr = 2aN\bar{n} \int_0^1 \tilde{n}^2 \tilde{r} d\tilde{r}. \tag{17}$$

Energy conserved during the compression is given by $pdV = dE$. Moreover, we can approximate the whole pdV work during a tiny axial compression of the spinning gas by applying the trapezoidal integral:

$$pdV \approx \frac{(\bar{p} + \bar{p}')(V - V')}{2}, \tag{18}$$

where $\bar{p}$, V and $\bar{p}'$, V' represent the axial pressures and volumes before and after the tiny compression, respectively. Three energies contribute to the total change in the system energy dE, whereas the conservation of energy during the compression is represented by:

$$\frac{(\bar{p} + \bar{p}')(V - V')}{2} = \Delta E_t + \Delta E_p + \Delta E_r, \tag{19}$$

where ΔE_t, ΔE_p, and ΔE_r correspond to the change in the thermal, potential, and rotational energies of the system during the tiny compression, respectively, which can be calculated individually using the formulas:

$$\Delta E_t = \frac{3}{2} N k_B (T' - T), \tag{20}$$

$$\Delta E_p = 2aN \left(\overline{n}' \int_0^1 \tilde{n}'^2 \tilde{r} d\tilde{r} - \overline{n} \int_0^1 \tilde{n}^2 \tilde{r} d\tilde{r} \right), \tag{21}$$

$$\Delta E_r = \frac{1}{2} M' \omega' - \frac{1}{2} M \omega. \tag{22}$$

Accordingly, we can find the value of T' and ω' after the tiny compression by solving the simultaneous equations of angular momentum (Equation (11)) and energy conservation (Equation (19)) using an iterative algorithm, as well as the distribution of $n(r)$ and axial pressure. Decomposing the continuous axial compression into a series of tiny compressions, we can generate a variation of the various physical quantities involved in the process through numerical calculations.

Here, we use the axial pressure ratio $\overline{p}_r/\overline{p}_s$, where $\overline{p}_r$ and $\overline{p}_s$ are the axial pressure of the spinning system and static system during the compression with the same initial T and $\overline{n}$, respectively, to qualitatively measure the increase in axial compressibility caused by the rotation of the gas. When $\overline{p}_r/\overline{p}_s < 1$, the axial compressibility of the spinning gas is larger than that of the static gas at the same compression ratio. Figure 1 illustrates the variation of $\overline{p}_r/\overline{p}_s$ during an adiabatic axial compression with different initial α_0, ξ_0, and φ_0.
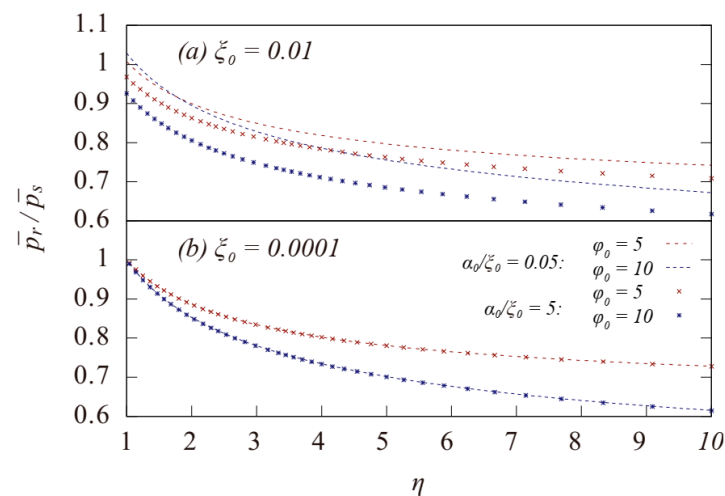
Figure 1. Variation of the pressure ratio of $\overline{p}_r$ to $\overline{p}_s$ during an adiabatic compression for a Van der Waals gas system with different initial ξ_0 and α_0. $\eta = \overline{n}/\overline{n}_0$ is the compression ratio. The red and blue dash line correspond to the results with $\alpha_0/\xi_0 = 0.05$ (weak attraction). The red and blue dots correspond to the result with $\alpha_0/\xi_0 = 5$ (strong attraction).

For all the curves listed in Figure 1, an axial pressure ratio of less than 1 can be achieved when the compression ratio η ($\eta = \overline{n}/\overline{n}_0$) is not too large. Moreover, it reaches about 0.6 at a large compression ratio, indicating that the effect of rotation-induced compressibility increase is very significant in our cases. In the case with $\xi_0 = 0.01$ and $\alpha_0/\xi_0 = 0.05$, the initial axial pressure ratio is greater than 1, implying that the rotation of the system increases the difficulty in axially compressing the gas in the initial situation. Nevertheless, this situation is reversed as η increases during a continuous compression. Figure 1 also suggests that a faster rotation speed (a larger value of φ_0) leads to smaller $\overline{p}_r/\overline{p}_s$ at the maximum compression ratio; thus, the rotation-induced compressibility increase becomes more significant as the system spins faster. The spinning gas becomes more compressible than static gas along the axis direction mainly because that part of the external pdV work

is converted into E_r during the axial compression, which slows down the temperature rise of the spinning gas as compared to that of the static gas, as shown in Figure 2.
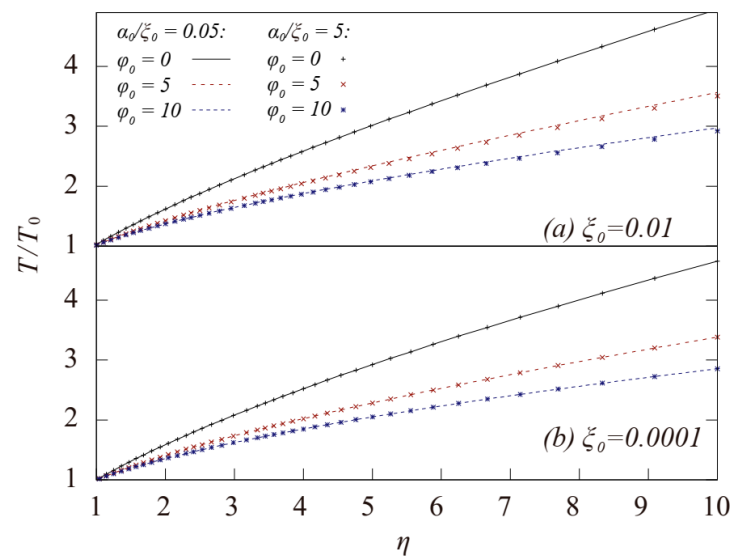
Figure 2. Variation of the temperature ratio of T to T_0 during an adiabatic compression of a Van der Waals gas system with different initial ξ_0 and α_0. T_0 is the initial temperature. The red and blue dash line correspond to the results with $\alpha_0/\xi_0 = 0.05$ (weak attraction). The red and blue dots correspond to the result with $\alpha_0/\xi_0 = 5$ (strong attraction).

Because the parameter α represents the attraction between the gas molecules, which is beneficial to the compression of the gas for both the spinning and static systems, it is evident in Figure 1 that a larger initial value of α_0 leads to a smaller $\bar{p}_r/\bar{p}_s$ at the maximum compression ratio, indicating that the attraction term in Van der Waals EOS can be more conducive to improving the axial compressibility of the gas in the spinning system. As illustrated in Figure 2, the curves of the temperatures with a larger α rise more slowly than those with a smaller α, which is consistent with the behavior of the axial pressure ratio. The attraction term in Van der Waals EOS is an^2; thus, the average attraction strength in a system with a nonuniform density distribution will be greater than that in a uniform system given the same average density. Additionally, it can explain the greater contribution of the attraction term in a spinning gas to the increase in the axial compressibility, because the rotation of the gas leads to a large degree of nonuniformity of density in radius.

3. Molecular Dynamics Simulations

The compressibility of gases is a common concern in high-energy-density physics, especially in the compression characteristics of gases (plasmas) under high-density conditions. As mentioned in the previous section, there are restrictions on the parameter range applicable to the Van der Waals EOS, which make this theoretical model inapplicable to understand the axial compressibility under high-density conditions. On the contrary, these parameter restrictions do not apply to MD methods, where more detailed dynamic processes in the gas compression can be considered. Thus, we employed the MD method to investigate the axial compression of a spinning Van der Waals gas and to further verify the robustness of the effect of rotation-induced compressibility increase in a system close to a real gas. Particularly, we applied the MD method, under the code LAMMPS [16], to simulate the axial compression of a spinning helium gas in a cylinder. The interaction potential between atoms utilized is the well-known Lennard–Jones (LJ) potential (LJ126 form):

$$V(r) = \varepsilon \left[\left(\frac{\sigma}{r} \right)^{12} - \left(\frac{\sigma}{r} \right)^{6} \right], \tag{23}$$

where $\varepsilon/k_B = 10.2$ K and $\sigma = 2.28$ Å [17].

To avoid the end effect and to satisfy the requirements of assumption (i) given earlier, we set a periodic boundary condition along the axis of rotation. Moreover, the interaction between the atoms and the sidewall of the cylinder was a short-range LJ potential to confine the atoms within the cylinder and to ensure that no friction would be applied on the atoms and the angular momentum of the system could be conserved.

We simulated the compression of the spinning gases in two different initial states to show the difference in the gas behavior near and away from an ideal gas state, which we will refer to as cases I and II. In case I, the initial mean number density was set to $\bar{n}_0 = 2.6875 \times 10^{25}$ m^{-3}, corresponding to a molar volume of 22.4 L under the standard state; initial temperature to $T_0 = 300$ K; and mass of the helium atom at $m = 4$ g/mol. Moreover, the cylinder had infinite length due to the boundary conditions. The height of the simulation cell was 1000 Å and contained 84,000 atoms. In case II, the initial mean mass density was set to $\rho = 0.125$ g/cm^3 (corresponding to $\bar{n}_0 = 7.525 \times 10^{28}$ m^{-3}), which is equal to the density of liquid helium, while the initial temperature was still $T_0 = 300$ K to ensure that the system was in a dense gas state. However, the cylinder had a radius $R = 100$ Å and a height $L_0 = 200$ Å and contained 120,000 atoms. In both cases, the maximum compression ratio was $\eta = 10$.

Here, we introduce the coupling factor $\Gamma = E_p/E_t$ to describe how far the gas deviates from the ideal gas. The value of Γ_0 and Γ_f, corresponding to the coupling factors of the system before and after compression, respectively, are shown in Table 1. Note that during the entire compression process of case I, Γ is very small, implying that the gas could be approximated as an ideal gas. In case II, however, the value of Γ varies greatly during the compression process, approaching 1 after compression, indicating that the potential energy of the interaction between the helium atoms is comparable to the kinetic energy of the thermal motion; thus, the gas is far from the ideal gas state.

Table 1. Parameters of the molecular dynamics (MD) simulations during the compression. $\Gamma = E_p/E_t$ is the coupling parameter of the gas, with Γ_0 and Γ_f corresponding to the coupling parameters of the initial and final state. Similarly, γ_p, γ_r and γ_t are the proportion of the changes in the potential energy ΔE_p, rotational energy ΔE_r and thermal energy ΔE_t, respectively, and correspond to the total pdV work during the whole compression.

	φ_0	Γ_0	Γ_f	γ_p (%)	γ_r (%)	γ_t (%)
Case I	0	1.58×10^{-5}	3.29×10^{-4}	0.04	0	99.96
	5	1.31×10^{-5}	3.96×10^{-4}	0.04	18.33	81.63
	10	6.15×10^{-5}	7.13×10^{-4}	0.07	31.76	68.13
	15	1.21×10^{-5}	1.11×10^{-4}	0.11	35.68	64.20
Case II	0	0.0112	0.750	44.74	0	55.26
	5	0.0283	0.823	45.17	4.82	50.01
	10	0.0219	0.927	42.66	16.34	40.99
	15	0.0996	1.012	39.05	27.12	33.83

The results of theoretical analysis suggest that $\varphi = m\omega^2 R^2/2k_B T$ is an important dimensionless parameter reflecting the spinning effect. To verify this, we conducted a series of simulations with different initial values of φ_0, with $\varphi = 0$ as a reference case.

Note that the density of the rotating system is not uniform under thermodynamic equilibrium. When a rotational angular velocity is applied to a static system in a thermodynamic equilibrium state, the atoms in the system will move outward under the action of a centrifugal force, causing the rise in the system temperature. Assuming that the temperature of the stationary system is T_0, the temperature rises to T_1 after the work of the centrifugal force reaches the thermodynamic equilibrium again. From a more comprehensive perspective, if we want to show that the compressibility of the gas is reduced

after it has entered the rotating state, we can opt to compare the difference between the static system of T_0 and the rotating system of T_1 in the compression process as a more reasonable solution than considering two systems with the same initial temperature. To maintain the same conditions as the previous work [8], we temporarily ignored the effect of the gas entering the rotating state process.

As the temperature of the system increased from the static to the rotating state, we needed to ensure that the system was balanced at the set temperature (300 K) after entering the rotating state in simulations. Thus, we followed this procedure in the simulations. First, we applied an equivalent centrifugal external field $\vec{F}_r = m\omega^2 \vec{r}$ to all atoms in the stationary system and used a nose-hoover heat bath [18] to allow the system to achieve equilibrium at 300 K under the centrifugal external field. Next, we removed the centrifugal external field and added a velocity component $\vec{v} = \vec{\omega} \times \vec{r}$ to the velocity component of each molecule to achieve the transition from a system under an equivalent centrifugal external field to a real spinning system, as illustrated in Figure 3. Because the radial density distribution of the spinning system is the same as that under an equivalent centrifugal external field, this transition process does not cause a change in temperature.
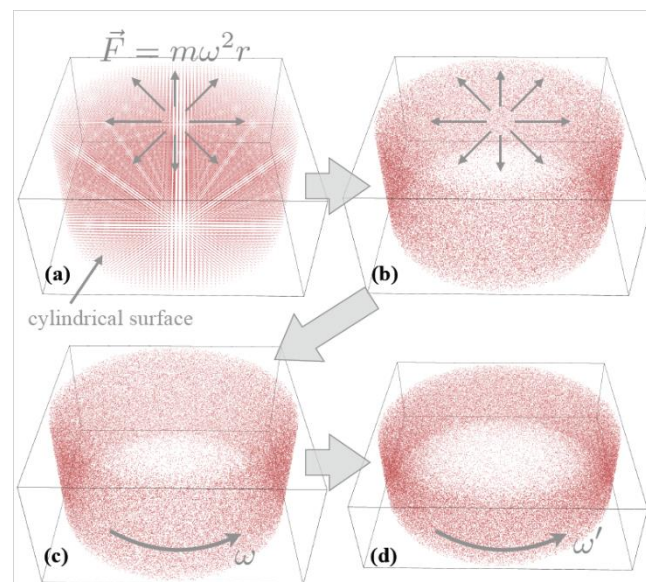

Figure 3. Schematic of MD simulations. (**a**) Initial lattice configuration of the atoms. (**b**) The thermodynamic equilibrium state under centrifugal external field. (**c**) The state-of-rotation equivalent to the centrifugal external field. (**d**) The state after a continuous compression.

As shown in Figure 4, the value of Γ in case I was very small; thus, the variation of pressure in the spinning system during the continuous compression process was similar to that of the ideal gas. A comparison of the curves would clarify that the value of $\overline{p}_r / \overline{p}_s$ in the MD simulations was lower than in the ideal gas, implying that the compressibility increase caused by rotation in the simulations was even larger than that of an ideal gas, especially for the cases with $\varphi_0 = 10$ and $\varphi_0 = 15$. This phenomenon could be attributed to the attraction term in the LJ potential.

Figure 5 shows a comparison of the variation of temperature of the MD simulations during the compression with different initial values of φ_0 in case I and that of the ideal gas model. For the static system ($\varphi_0 = 0$), the temperature of MD system rose faster than that of the ideal gas system, suggesting that a larger proportion of the pdV work used to overcome the virial pressure p_v during the compression has been converted into the thermal energy E_t. By contrast, the temperature rises in the MD simulations for the cases with $\varphi_0 = 10$ and $\varphi_0 = 15$ was less than that of the ideal gas model. As a result, the value of $\overline{p}_s$ in the static system, used as a reference value in Figure 4, was larger in the MD simulations than

in the stationary ideal gas, whereas $\overline{p}_r/\overline{p}_s$ in the simulations were lower than in the ideal gas system.
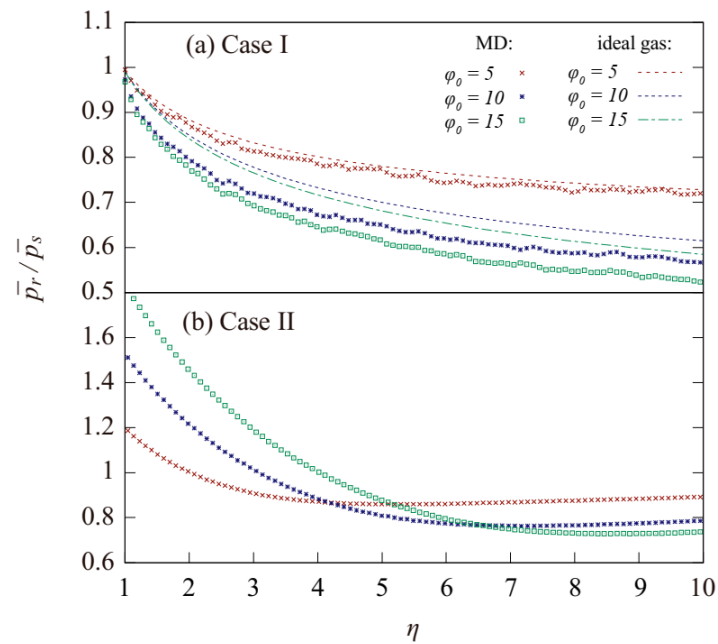
Figure 4. Variation of the pressure ratio $\overline{p}_r$ to $\overline{p}_s$ during an adiabatic compression with different initial φ_0 in the MD simulations. $\eta = \overline{n}/\overline{n}_0$ is the compression ratio. The red, blue, and green dash line correspond to the results in ideal gas. The red, blue, and green dots correspond to the result obtained with MD simulations.
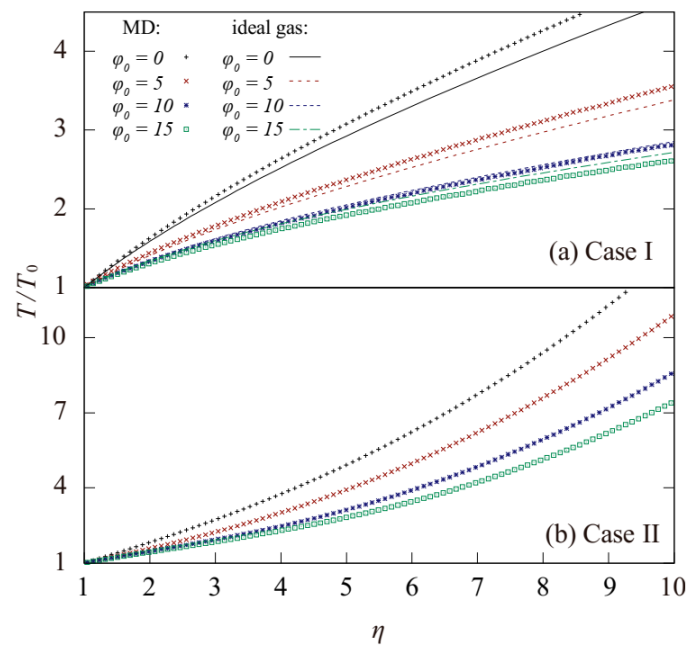
Figure 5. Variation of the temperature ratio T to T_0 during an adiabatic compression with different initial φ_0 in the MD simulations. T_0 is the initial temperature. The red, blue, and green dash line correspond to the results in ideal gas. The red, blue, and green dots correspond to the result obtained with MD simulations.

As also depicted in Figure 4, the initial pressure increase caused by the rotation was very obvious in case II. Here, a larger value of φ_0 corresponded with a larger initial pressure

ratio $\overline{p}_r / \overline{p}_s$. Moreover, as the value of η increased, the $\overline{p}_r / \overline{p}_s$ of the systems with a larger φ_0 decreased at a faster rate and eventually exceeded those for the systems with a smaller φ_0, which resulted in a smaller $\overline{p}_r / \overline{p}_s$ similar to that for the virial gas model [9].

The variation of temperature in case II is shown in Figure 5. Larger values of the initial φ_0 resulted in a slower temperature rise during the compression, similar to other cases mentioned in this work, except that the proportion of the system temperature increase T/T_0 during compression was much higher. As η reached 10, T/T_0 was lower than 5 for the stationary ideal gas, whereas it was larger than 10 in case II with $\varphi_0 = 0$ and $\varphi_0 = 5$, mainly because a large part of the pdV work overcoming the virial pressure during compression was converted to E_t for the gas systems having E_p comparable to E_t, which accelerated the increase in the temperature during compression. Generally speaking, the potential energy of the system showed a very strong nonlinear relationship with the thermodynamic parameters of the system, which entails that the presence of potential energy in nonideal gases will lead to unpredictable behavior of the system during compression.

The energy conversion relationship during the entire compression process is shown in Table 1. Note that, as the value of φ_0 increased, the proportion of the pdV work converted to the rotational energy γ_r increased incrementally, whereas the proportion converted to thermal energy γ_t decreased incrementally, making the compressibility reduction caused by rotation more pronounced. Moreover, the proportion of the pdV work converted to potential energy γ_p did not change much with the change of φ_0 for both cases I and II.

4. Summary

We applied the theoretical analysis and MD methods to investigate the axial compression of a spinning Van der Waals gas in a smooth cylinder. Based on the analytical results and MD calculations, the Van der Waals gas exhibited a rotation-induced compressibility increase effect during a continuous axial compression; the primary reason is that the temperature of the spinning gas rising more slowly than that of the stationary gas. We also found that the attraction term in the Van der Waals EOS had a significant contribution to the axial compressibility increase in the spinning system. Moreover, our MD simulations for a spinning gas with a large coupling factor Γ showed that the increase effect of the rotation-induced compressibility remained significant even when the gas state was far from the ideal gas state, which further illustrates the robustness of this effect. The robustness of this effect indicates that it is likely to be observed in experiments. Furthermore, this effect can be applied in many fields where high compression of gas or plasmas is required, such as Z-pinch experiments. The facility of Z-pinch experiments is a cylinder. The increase in compressibility is helpful to achieve the experimental goal of compressing high-temperature plasma to an extremely high density and areal density.

In the theoretical analysis and simulation of this work, the assumptions adopted are difficult to realize under a real compression of real gas. The effects of non-equilibrium dynamics during a non-quasi-static compression, wall friction and non-adiabatic process on the experimental results should be taken into consideration in further investigations.

Appendix A

Table A1. The list of definitions and expressions of all parameters.

Parameter	Definition	Expression
p	pressure	
n	the number density	
T	temperature	
k_B	Boltzmann constant	
a	coefficient of the weak attraction term in Van der Waals EOS	
b	coefficient of the molecular volume modification in Van der Waals EOS	
m	mass of a gas molecule	
ω	the angular speed	
r	the dimensionless radius	
N	the total number of particles	
$\bar{n}$	the mean number density	$\frac{N}{pR^2L}$
$\tilde{n}$	the dimensionless number density	$\frac{n}{\bar{n}}$
$\tilde{r}$	the cylindrical radius	$\frac{r}{R}$
α	the dimensionless parameter describing the ratio of the attractive interaction energy to the thermal energy of the system	$\frac{2a\tilde{n}}{k_BT}$
ζ	the dimensionless parameter describing the strength of molecular repulsion potential	$b\bar{n}$
φ	the dimensionless parameter describing the ratio of the spinning kinetic energy to the thermal energy	$\frac{m\omega^2R^2}{2k_BT}$
V	the volume of the cylinder	
R	the radius of the cylinder	
L	the height of the cylinder	
M	the angular momentum	
U	the internal energy	
C_V	the isometric heat capacity	$\left(\frac{\partial U}{\partial T}\right)_V$
ΔE_t	the change in the thermal energy	
ΔE_p	the change in the potential energy	
ΔE_r	the change in the rotational energy	
$\bar{p}_r$	the axial pressures of the spinning system	
$\bar{p}_s$	the axial pressures of static system	
$\bar{n}_0$	the initial mean number density	
η	the compression ratio	$\frac{\bar{n}}{\bar{n}_0}$

References

1. He, X.; Li, J.; Fan, Z.; Wang, L.; Liu, J.; Lan, K.; Wu, J.; Ye, W. A hybrid-drive nonisobaric-ignition scheme for inertial confinement fusion. *Phys. Plasmas* **2016**, *23*, 82706. [CrossRef]
2. Li-Feng, W.; Jun-Feng, W.; Wen-Hua, Y.; Zheng-Feng, F.; Xian-Tu, H. Design of an Indirect-Drive Pulse Shape for ~1.6 MJ Inertial Confinement Fusion Ignition Capsules. *Chin. Phys. Lett.* **2014**, *31*, 45201.

3. Wang, F.; Li, Y.-L.; Wang, Z.-B.; Xu, T.; Zha, W.-Y.; Yang, D. Demonstration of a Shock-Timing Experiment in a CH Layer at the ShenGuang III Laser Facility. *Chin. Phys. Lett.* **2018**, *35*, 55202. [CrossRef]
4. Yu, C.; Wu, S.; Yang, W. Theoretical investigation of gas filling and leaking in inertial confinement fusion hohlraum. *Sustainability* **2018**, *10*, 3763. [CrossRef]
5. Drake, R.P. *High-Energy-Density Physics: Foundation of Inertial Fusion and Experimental Astrophysics*; Springer: Cham, Switzerland, 2006.
6. Ye, H.; Lai, H.; Li, D.; Gan, Y.; Lin, C.; Chen, L.; Xu, A. Knudsen Number Effects on Two-Dimensional Rayleigh-Taylor Instability in Compressible Fluid: Based on a Discrete Boltzmann Method. *Entropy* **2020**, *22*, 500. [CrossRef] [PubMed]
7. He, S.-K.; Jiao, J.-L.; Deng, Z.-G.; Lu, F.; Yang, L.; Zhang, F.-Q.; Dong, K.-G.; Hong, W.; Zhang, Z.-M.; Zhang, B.; et al. Generation of Ultrahigh-Velocity Collisionless Electrostatic Shocks Using an Ultra-Intense Laser Pulse Interacting with Foil-Gas Target. *Chin. Phys. Lett.* **2019**, *36*. [CrossRef]
8. James, R.A. The Structure and Stability of Rotating Gas Masses. *Astrophys. J.* **1964**, *140*, 552. [CrossRef]
9. Lebedev, S.V.; Mitchell, I.H.; Aliaga-Rossel, R.; Bland, S.N.; Chittenden, J.P.; Dangor, A.E.; Haines, M.G. Azimuthal Structure and Global Instability in the Implosion Phase of Wire Array Z-Pinch Experiments. *Phys. Rev. Lett.* **1998**, *81*, 4152. [CrossRef]
10. Harvey-Thompson, A.J.; Lebedev, S.V.; Burdiak, G.; Waisman, E.M.; Hall, G.N.; Suzuki-Vidal, F.; Bland, S.N.; Chittenden, J.P.; De Grouchy, P.; Khoory, E.; et al. Suppression of the ablation phase in wire array Z pinches using a tailored current prepulse. *Phys. Rev. Lett.* **2011**, *106*, 205002. [CrossRef] [PubMed]
11. Sousa, J.; Paniagua, G.; Collado Morata, E. Thermodynamic analysis of a gas turbine engine with a rotating detonation combustor. *Appl. Energy* **2017**, *195*, 247–256. [CrossRef]
12. Geyko, V.I.; Fisch, N.J. Compressibility and heat capacity of rotating plasma. *Phys. Plasmas* **2017**, *24*. [CrossRef]
13. Geyko, V.I.; Fisch, N.J. Reduced compressibility and an inverse problem for a spinning gas. *Phys. Rev. Lett.* **2013**, *110*, 150604. [CrossRef] [PubMed]
14. Zhang, Y.-W.; Su, S.-L.; Xie, S.-B.; Zhou, W.-M.; Liu, H. Investigation into the improved axial compressibility of a spinning non-ideal gas. *Front. Phys.* **2020**, *15*. [CrossRef]
15. Liu, H.; Kang, W.; Zhang, Q.; Zhang, Y.; Duan, H.; He, X.T. Molecular dynamics simulations of microscopic structure of ultra strong shock waves in dense helium. *Front. Phys.* **2016**, *11*, 115206. [CrossRef]
16. Plimpton, S. Fast Parallel Algorithms for Short-Range Molecular Dynamics. *J. Comput. Phys.* **1995**, *117*, 1–19. [CrossRef]
17. Allen, M.P.; Tildesley, D.J. *Computer Simulation of Liquids*; Oxford University Press: New York, NY, USA, 1989.
18. Nosé, S. A unified formulation of the constant temperature molecular dynamics methods. *J. Chem. Phys.* **1984**, *81*, 511–519. [CrossRef]